

Radar backscatter from plasma irregularities of the lower E region induced by neutral turbulence

K. Schlegel, A. V. Gurevich¹

Max-Planck-Institut für Aeronomie, 37189 Katlenburg, Lindau, Germany

Received: 1 April 1996/Revised: 2 July 1996/Accepted: 3 July 1996

Abstract. Recently, one of the authors (A. V. G.) developed a theory of low-frequency plasma irregularities which are created as a consequence of neutral turbulence in the D and lower E regions. In the following this theory will be applied to coherent backscatter experiments with radars in a frequency range between 5 and 150 MHz. We discuss the dependence of the backscatter cross-section on ionospheric as well as on turbulence parameters. The backscatter increases strongly with decreasing radar frequency. Above 15 MHz the effects discussed here can probably only be detected by very powerful radars with large antenna arrays.

1 Introduction

Plasma turbulence in the ionospheric E region is well explored mainly through radar backscatter experiments (for reviews see e.g. Schlegel, 1996; Haldoupis, 1989) or rocket experiments (e.g. Rose *et al.*, 1992; Pfaff, 1991). It is usually attributed to plasma instabilities like the modified two-stream or Farley-Buneman instability (Farley, 1963; Buneman, 1963) and the gradient drift instability (Simon, 1963). These instabilities are excited in the altitude range of about 100–120 km. Below this region both instabilities are severely damped due to the increasing number of collisions between the plasma particles and neutrals. Unstable plasma waves, however, have also been detected well below 100 km, mainly by rocket experiments (e.g. Blix and Thrane, 1996; Blix *et al.*, 1994; Rinnert, 1992; Schlegel, 1992; Pfaff, 1991; Røyrvik and Smith, 1984), indicating that mechanisms other than the mentioned plasma instabilities are responsible for the plasma turbulence.

Gurevich *et al.* (1996) recently developed a new theory which describes quantitatively the transfer of neutral

turbulence to a plasma, resulting in low-frequency plasma irregularities. They assume Kolmogorov's “ $-5/3$ -law” for the neutral turbulence and characterize it further by three parameters, namely the energy dissipation rate ε , the characteristic velocity V_0 and a characteristic scale l_0 . It is further assumed that the turbulent structures of the neutral density cause in turn irregularities in the electron density which can be detected by a suitable radar. The characteristics of the electron density structures are mainly determined by the turbulence parameters just given for altitudes below about 90 km because of the frequent collisions between the electrons and neutrals. At greater heights the electron density structures are in addition influenced by plasma processes, particularly by the different electron mobility parallel and perpendicular to the geomagnetic field lines, introducing an aspect sensitivity of the radar return. Gurevich *et al.* (1996) calculated the electron density fluctuations as well as the electric field fluctuations as a function of frequency and wave number, using a quasi-neutral fluid theory approximation. One of their results is an analytical formula for radar backscatter. This cross-section is quantitatively explored in the following, and the implications for backscatter experiments in the MF, HF and VHF ranges are discussed.

In principle this new theory should also be applicable to mesospheric backscatter. For the first time it provides an explicit expression for the spectral shape, which was not available in previous theoretical approaches. A detailed discussion in terms of mesospheric applications (e.g. MST radars) however, is beyond the scope of this contribution. We are concentrating here on the height range of the lower E region.

The paper is organized as follows: in Sect. 2 the cross-section formula is explained in detail; its height dependence is discussed in Sect. 3. Section 4 discusses the spectral shape and the dependence on various plasma parameters and Sect. 5 gives estimates of the actual backscattered power for an experiment with an assumed antenna configuration. Section 6 concludes the paper.

¹ On leave from P. N. Levedev Institute of Physics, 117924 MOSCOW
Correspondence to: K. Schlegel

2 Analytical form of the backscatter cross-section

From the theory of Gurevich *et al.* (1996), an expression for the differential Doppler spectrum of the radar backscatter can be developed. The corresponding radar backscatter cross-section per unit frequency and per unit solid angle Ω reads:

$$\begin{aligned} & \left(\frac{d^2\sigma}{d\Omega d\omega} \right)_k, \\ &= \frac{e^4 R^2 \varepsilon^{2/3}}{3m^2 c^4 k^3 V_0 \omega_H^2 \sin \beta} \exp \left\{ - \frac{(\omega - \vec{k} \cdot \vec{v}_{n0})^2}{k^2 V_0^2} \right\} \\ & \times \int \frac{l_0^{5/3} v_{en}^2 N_0^2 (1+y^2) y^2 k_{perp}^2 E(x) dz}{[1 + \Psi_{perp}(1+y^2)]^2 [(\omega - \vec{k} \cdot \vec{v}_{n0} - \omega_0)^2 + \gamma^2]}, \end{aligned} \quad (1)$$

with the following constants: e = elementary charge, m = electron mass, c = speed of light, and parameters: R = range to scattering volume, ε = energy dissipation rate of the neutral turbulence, k = wave vector of irregularities ($= 4\pi f_{radar}/c$), V_0 = characteristic velocity of turbulence, ω_H = electron gyro frequency, β = elevation angle of radar line of sight, v_{n0} = neutral wind velocity, v_{en} = electron neutral collision frequency and $N_0(z)$ = electron density.

The characteristic scale of turbulence can be expressed according to Tatarski (1961):

$$\begin{aligned} l_0 &= 1.8 \cdot 10^3 \left(\frac{10^{13} \text{ cm}^{-3}}{N_n(z)} \right)^{3/4} \left(\frac{T(z)}{240 \text{ K}} \right)^{3/8} \\ & \times \left(\frac{\varepsilon}{10^3 \text{ cm}^2 \text{ s}^{-3}} \right)^{-1/4} \quad [\text{cm}]. \end{aligned} \quad (2)$$

$N_n(z)$ is the neutral density in cm^{-3} and $T(z)$ the neutral temperature in Kelvin. Both are functions of altitude z , whereas for the energy dissipation rate ε a mean value valid for the whole altitude range 70–110 km is assumed.

With the help of l_0 a universal energy spectrum of the turbulence can be defined (Sirovich *et al.*, 1994):

$$E(x) = (1.14x^{-5/3} + 0.626x^{-1}) \exp(-0.57x) \quad x = kl_0; \quad (3)$$

for $x < 1$ this spectrum reduces to the well-known Kolmogorov law, for larger x it falls off exponentially.

Further expression characterize the plasma and its interaction with the neutrals via collisions:

$$y = \frac{k_{par}}{k_{perp}} \frac{\omega_H}{v_{en}(z)}, \quad k^2 = k_{par}^2 + k_{perp}^2, \quad (4)$$

$$\Psi_{perp} = \frac{v_{en}(z)v_{in}(z)}{\omega_H M \Omega_H}, \quad \Omega_H = \frac{m}{M} \omega_H, \quad (5)$$

where M is neutral mass and v_{in} ion neutral collision frequency. The linear phase velocity of the plasma waves is defined as usual:

$$\omega_0 = \vec{k} \cdot \vec{v}_d / (1 + \Psi), \quad \vec{v}_d = \vec{v}_e + \psi \vec{v}_i,$$

$$\psi = \Psi_{perp} (1 + y^2) \frac{k_{perp}^2}{k^2}, \quad (6)$$

where v_e and v_i are electron and ion drift velocity, respectively. The damping of the unstable waves is assumed to result from collisions (through ψ) and from diffusion:

$$\gamma = \frac{2k_{\perp}^2 D_{e\text{perp}}(1+y^2)}{1+\psi}, \quad D_{e\text{perp}} = \frac{T(z)v_{en}(z)}{m\omega_H^2}. \quad (7)$$

If not otherwise specified, a ‘standard set’ of parameters has been used in the following calculations: $f_{radar} = 10 \text{ MHz}$, $\varepsilon = 0.1 \text{ W kg}^{-1} = 1000 \text{ cm}^2 \text{ s}^{-3}$, $V_0 = 10 \text{ m s}^{-1}$, $\omega_H = 0.88 \cdot 10^7 \text{ s}^{-1}$, $v_{n0} = 30 \text{ m s}^{-1}$, $v_e = v_d = 40 \text{ m s}^{-1}$ ($v_i = 0$) and $k_{par} = 0.01 k_{perp}$. For simplicity it was assumed that v_{n0} and v_e are directed along the radar wave vector.

The values for ε and V_0 are taken from Hocking (1990), and seem to be typical for strong turbulence (see the discussion in Sect. 4c, e), and v_{n0} from Manson *et al.* (1990). The relation $k_{par}/k_{perp} = 0.01$ indicates an aspect angle (angle between the radar wave vector and the normal of the magnetic field direction) of 0.57° , i.e. almost perpendicular. It has been assumed that the radar is located at mid-latitudes and the radar elevation angle has therefore been taken as $\beta = 30^\circ$, resulting in a range to the scattering volume $R = 180 \text{ km}$ if its mean height is around 90 km .

3 Height variation of parameters

First of all, it is useful to consider the variation of some of the input parameters with altitude. Such an overview is shown in Fig. 1 for the neutral temperature, the neutral density, the electron and ion collision frequency, the perpendicular diffusion coefficient, the parameter Ψ_{perp} , the scale of the neutral turbulence and the electron density. The values of T_n , N_n and N_0 have been taken from Appendix B of Kelley (1989), v_{en} and v_{in} have been calculated from these data with the help of formulas given in the same publication; the other parameters have been calculated from the equations given in Sect. 2. It is obvious that all of these parameters, except the neutral temperature, vary over several orders of magnitude in the height range of 70 to 110 km. A large change in the scattering cross-section with altitude can therefore be expected.

In order to bracket the height range which is important for the calculation of the differential cross-section, the integrand of Eq. 1 [in the following called $I(\omega)$] was examined for different heights as a function of Doppler frequency. $I(\omega)$ constitutes a Lorentzian-shaped function (second bracket in the denominator) in terms of ω . Its width is determined by γ , the damping of the plasma waves. Since γ increases with altitude (mainly because of the decrease in ψ), $I(\omega)$ becomes broader with increasing height. The centre of $I(\omega)$ is solely determined by the neutral wind velocity v_{n0} at low heights. At greater heights the influence of the electron drift velocity v_e (through ω_0) becomes important. The magnitude of $I(\omega)$ is controlled by the turbulent energy density $E(x)$. Since $x = kl_0$ is already strongly height dependent (see Fig. 1), $E(x)$ varies over 27 orders of magnitude between 70- and 110-km

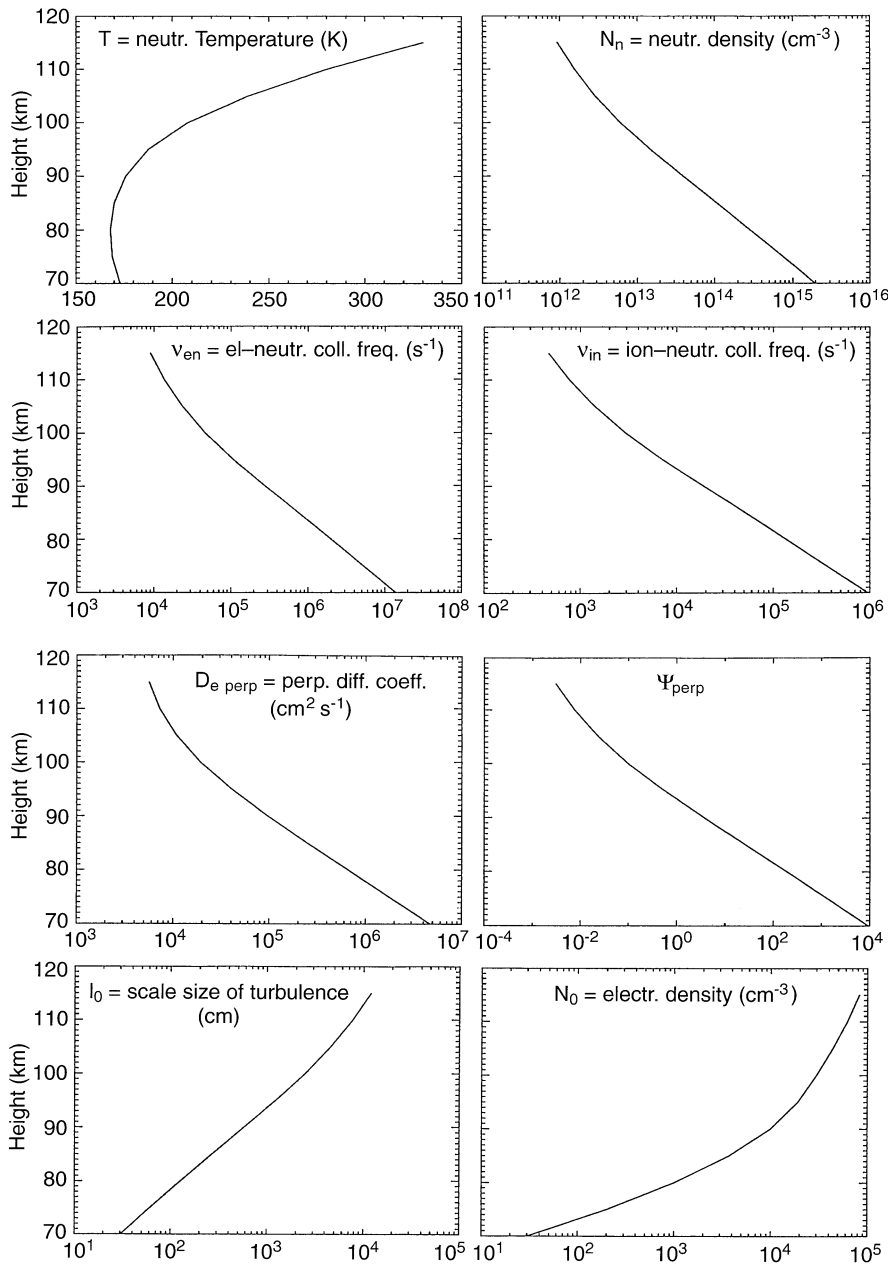


Fig. 1. Height variation of important parameters which enter the backscatter cross-section (Eq. 1)

altitude. The location of the maximum in the height profile of $I(\omega)$ also depends on the radar wavelength (through $x = 2\pi l_0/\lambda$). This maximum altitude and the height profile of $E(x)$ therefore define the height range over which the integration in Eq. 1 has to be taken. We used

- for 5 MHz: $85 < z < 114$ km,
 - for 10 MHz: $80 < z < 108$ km,
 - for 50 MHz: $75 < z < 99$ km,
 - for 150 MHz: $70 < z < 89$ km.
- (8)

Outside these intervals the contribution of $I(\omega)$ to the integral in Eq. 1 is negligible [$I(\omega)/I_{\max}(\omega) < 10^{-4}$]. The

detailed behaviour of $I(\omega)$ is documented in Schlegel and Gurevich (1995).

4 Discussion of backscatter cross-section

4.1 Differential and total cross-section

Figure 2 shows backscatter spectra for different radar frequencies. In order to facilitate a better comparison, they have been plotted versus Doppler velocity rather than Doppler frequency. In addition they have been normalized to unity. The values printed in the upper left-hand corner of each panel give the radar frequency and the total

cross-section per unit solid angle, i.e. the integral

$$\frac{d\sigma}{d\Omega} = \int \left(\frac{d^2\sigma}{d\Omega d\omega} \right) d\omega. \quad (9)$$

It is interesting to note that the mean Doppler velocity decreases with increasing radar frequency. This is due to the fact that the mean Doppler velocity in the spectra results from a superposition of the neutral velocity v_{n0} and the $\mathbf{E} \times \mathbf{B}$ drift v_d . At smaller radar frequencies the integration interval (see (8)) shifts to greater heights where the influence of v_d increases, thus leading to higher mean Doppler velocities. This effect is demonstrated clearly in the spectrum for 5 MHz (upper left-hand panel of Fig. 2), where the contributions from height steps above 105 km (separated by 1 km in our calculations) introduce spikes in the upper half of the spectrum. Consequently, the spectra become more symmetric with increasing radar frequency.

Again it can be seen that the total cross-section is strongly dependent on the radar frequency. This is even more evident from Fig. 3, where the total cross-section is plotted versus radar frequency. It decreases by 15 orders of magnitude between radar frequencies of 4 and

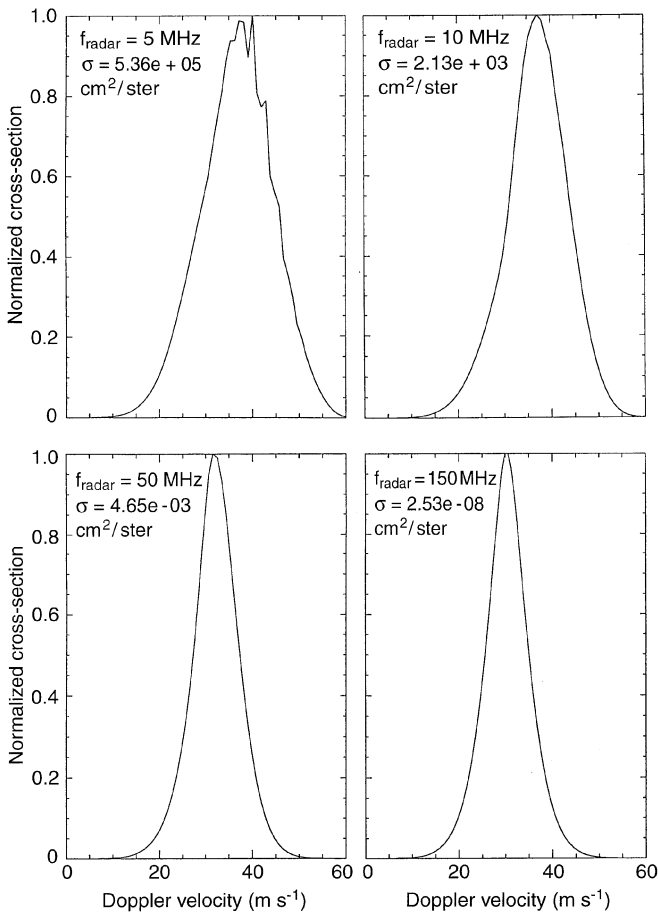


Fig. 2. Normalized differential cross-section as a function of Doppler velocity for four different radar frequencies as printed on top of each panel; σ is the cross-section per unit solid angle obtained by integrating Eq. 1 with respect to ω , (Eq. 9)

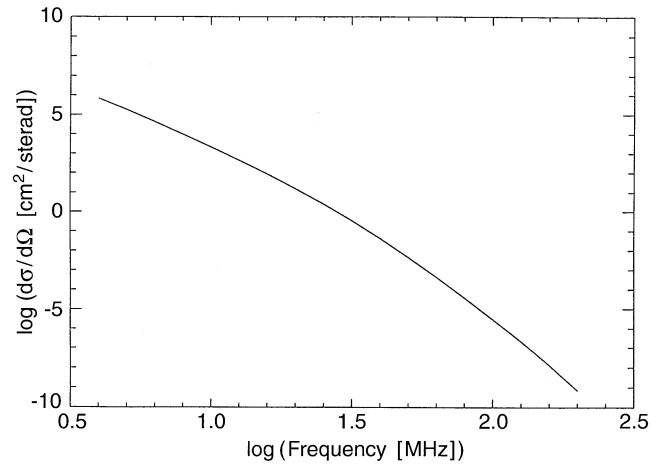


Fig. 3. Cross-section per unit solid angle as a function of radar frequency

200 MHz. The detectability of such echoes will be discussed in Sect. 5.

4.2 Influence of neutral wind and $\mathbf{E} \times \mathbf{B}$ drift

The interplay of neutral wind and $\mathbf{E} \times \mathbf{B}$ drift in the determination of the mean Doppler shift of the spectra is easily understood from Eq. 1. The ‘standard’ spectrum for 10 MHz (upper right-hand panel of Fig. 2) shows a mean Doppler shift of 37 m s^{-1} . This is the sum of the ‘standard’ neutral wind velocity $v_0 = 30 \text{ m s}^{-1}$ and the ‘standard’ $\mathbf{E} \times \mathbf{B}$ drift $v_0 = 40 \text{ m s}^{-1}$ leading to $\omega_0/k \approx 7 \text{ m s}^{-1}$. For the other three radar frequencies the mean Doppler shift can be understood in a similar way.

In the standard parameter set we have so far always applied a neutral wind velocity which was constant in altitude, a case which is quite unrealistic in practice. We have therefore examined the influence of a wind profile on the spectrum. All the other parameters have been kept from the standard set. Basically, two details are different in this case: the mean Doppler velocity corresponds to the wind velocity at the height of the maximal contribution of $I(\omega)$ to the integral in Eq. 1, which is about 95 km for the radar frequency of 10 MHz; and the width of the spectrum is about 60–70% greater than the width of the standard case, depending mainly on the gradient of the wind in the vicinity of the height of maximal contribution.

Different values of the $\mathbf{E} \times \mathbf{B}$ drift have only a very small influence on the mean Doppler velocity of the spectrum, at least for a radar frequency above 10 MHz. This influence increases for smaller radar frequencies however, due to the fact that in this case the integration interval of Eq. 1 has to be shifted to greater heights, where, in turn, ψ is smaller and thus the influence of ω_0 stronger, as already mentioned. The $\mathbf{E} \times \mathbf{B}$ influence on the spectrum decreases strongly if the radar beam is moved away from the aspect angle around 0° . In this case k_{par} and in turn y and ψ increase (Eqs. 4 and 6), yielding very small values of ω_0 . We actually used the small aspect angle in our

'standard' case in order to demonstrate the $\mathbf{E} \times \mathbf{B}$ influence, although the chosen geometry may be difficult to achieve with large antennas (see Sect. 5).

4.3 The width of the spectrum

The width of the backscatter cross-section (Eq. 1) is determined by two parameters: the characteristic velocity of the turbulence V_0 and the damping of the waves γ (Eq. 7). The variation of V_0 in the atmosphere is not well known, values of the order of 10 m s^{-1} as obtained from radar measurements (Hocking, 1990) are probably typical for strong turbulence. Average values of the order of 1 m s^{-1} as obtained from in situ rocket data seem to be more common (Lübken *et al.*, 1993). A similar uncertainty of about a factor of two exists for γ due to variations in the neutral temperature and the neutral density (and in turn in the electron-neutral collision frequency). It should be stressed again, however, that the influence of γ on the width of the spectrum is only important at heights above 95 km, which contribute to the height integral, Eq. 1, only for low radar frequencies. It should further be noted that the width dependence on V_0 leads to Gaussian-shaped spectra, the width dependence on γ to Lorentzian-shaped spectra. A differentiation of measured spectra between these two types is possible, as the work of Hanuise *et al.* (1993) has shown.

A width of a few 10 m s^{-1} , which our calculations reveal, is much lower than the spectral width usually measured by coherent or auroral radars at frequencies between 50 and 150 MHz. Width values of the order of 100 m s^{-1} or more quite normal (e.g. Schlegel *et al.*, 1986). With the present theory such broad spectra can only be explained by unrealistically high wind variations over the altitude range relevant for the height integration of Eq. 1, together with variations in V_0 and the other neutral gas properties. It should be kept in mind however, that auroral radars are usually sensitive to an altitude range of 95–115 km, which is higher than the ranges regarded in this study for 50–150 MHz (see Sect. 3). The situation is different for MF-radar results where the measured width values are comparable to those obtained here (Schlegel *et al.*, 1978, see Sect. 6).

4.4 Influence of the aspect angle

The aspect angle, that is the angle between the radar wave vector and the normal of the geomagnetic field direction, has quite a strong influence on the shape as well as on the total backscatter cross-section. This is true however, only for radar frequencies at 10 MHz and below, because the $\mathbf{E} \times \mathbf{B}$ influence is almost negligible at radar frequencies above 10 MHz, as already stated in Sect. 4.2.

Since the aspect angle α is defined as

$$\tan \alpha = k_{\text{par}}/k_{\text{perp}}, \quad (10)$$

it is the parameter y (Eq. 3) which is affected here, and which enters Eq. 1 in various terms. Figure 4a shows the total cross-section (Eq. 9) for 10 MHz as a function of

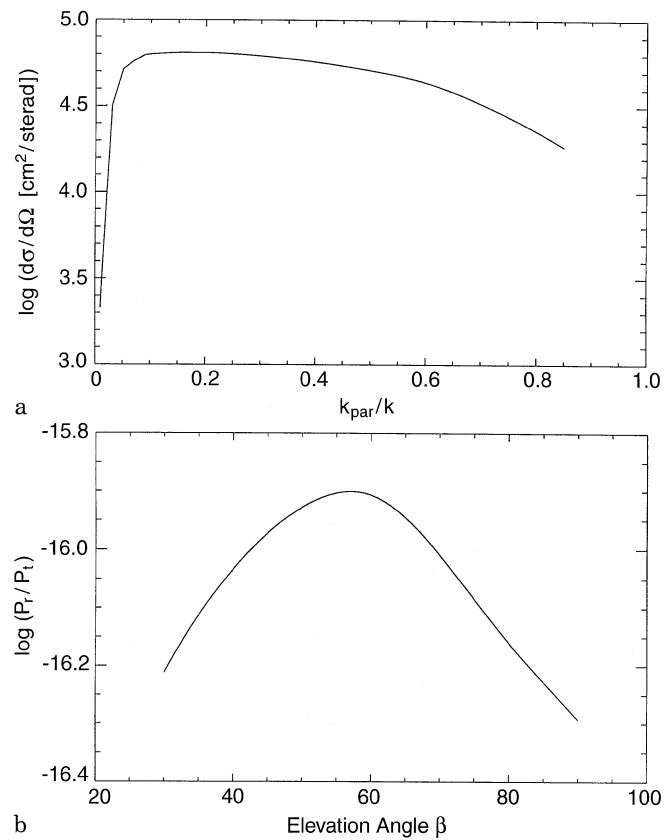


Fig. 4. **a** Cross-section per unit solid angle as a function of the aspect angle α , expressed as the ratio $k_{\text{par}}/k = \sin \alpha$ for a radar frequency of 10 MHz. **b** Backscattered power ratio P_r/P_t as a function of radar elevation angle for 10 MHz

$\sin \alpha = k_{\text{par}}/k$. The standard case, $k_{\text{par}}/k = 0.01$, corresponds to the left starting point of the two curves. It is clear from Eq. 1 that the cross-section is zero for $k_{\text{par}} = 0$, because it means $y = 0$. The cross-section increases up to a value of $k_{\text{par}}/k \approx 0.1$ ($\alpha \approx 6^\circ$) by a factor of 40. For larger aspect angles the cross-section weakly decreases again. It should be noted that in these calculations all other parameters have been kept to the standard set. This is quite unrealistic in practice with respect to R and β (Eq. 1) and to neutral wind and $\mathbf{E} \times \mathbf{B}$ drift, which all change their values if the radar beam is more elevated. We have nevertheless kept these parameters constant in order to investigate the sole influence of the aspect angle. A more detailed discussion of the influence of the radar elevation angle as shown in Fig. 4b follows in Sect. 5.

4.5 Influence of the energy dissipation rate

Whereas the characteristic velocity V_0 influences mainly the width of the spectra, it is interesting to examine the influence of the energy dissipation rate ε which enters Eq. 1 directly and via l_0 (Eq. 2). We are aware that this parameter shows strong natural fluctuations and varies at least by a factor of 5 in the height range in question. Recent rocket results (Lübken *et al.*, 1993) indicate that

ε can be smaller by a factor of 10 compared to previous radar estimates (Hocking, 1990). The calculations show that the total backscatter cross-section increases by a factor of about 3 when ε is increased by a factor of 5. This ratio is almost independent of the radar frequency.

5 The backscatter power spectrum

In order to study the effects of a variation of the radar elevation angle more realistically, the total backscattered power spectrum has been calculated. The backscattered power as a function of frequency can be expressed as:

$$P_r(\omega) = P_t \frac{\lambda_{\text{radar}}^2}{(4\pi R^2)^2} \int S(\omega, \vartheta, \varphi) G_t(\vartheta, \varphi) G_r(\vartheta, \varphi) d\vartheta d\varphi, \quad (11)$$

with

$$S(\omega, \vartheta, \varphi) = \left(\frac{d^2 \sigma}{d\Omega d\omega} \right)_{\vec{k}}, \quad d\Omega = d\vartheta d\varphi. \quad (12)$$

$G_t(\vartheta, \varphi)$ and $G_r(\vartheta, \varphi)$ are the gain of the transmitting and receiving antenna, respectively, P_t is the transmitted power and ϑ and φ are the angles spanning the plane perpendicular to \vec{k} . These angles enter the cross-section (Eq. 1) via the scalar products $\vec{k} \cdot \vec{v}_{no}$ and $\vec{k} \cdot \vec{v}_d$, as well as through the aspect angle.

We have used a model antenna for this calculation corresponding to the electric properties of the antenna built for the HEATING project near Tromsø (Stubbe *et al.*, 1982). It has a beam half-width of 7.25° in both dimensions (ϑ and φ) and a total gain of 24 db, and can be realised by an array of 6×6 dipoles. It is used in our case for transmitting and receiving. The gain factors can be expressed as

$$G_t(\vartheta, \varphi) = G_r(\vartheta, \varphi) = g_0 \exp\left(\frac{\vartheta^2 + \varphi^2}{w^2 / \log(2)}\right), \quad (13)$$

with $g_0 = 251.2$ and $w = 7.25^\circ$.

We have first kept the radar elevation of $\beta = 30^\circ$ and all the parameters of the standard set (neutral wind constant with height) and calculated the integral Eq. 11 although we are aware that this beam elevation may be difficult to achieve with such an antenna. The result shows that the form of this power spectrum is very similar to the form of the cross-section spectrum (upper right-hand panel of Fig. 2), mean Doppler velocity and width are almost the same. The ratio of received to transmitted power after integrating over the whole spectrum with respect to ω is $P_r/P_t = 6.14 \cdot 10^{-17}$.

It is also interesting to inspect the integrand of Eq. 11, i.e. the backscatter cross-section folded with the antenna pattern. It is displayed in Fig. 5a, from which it can be seen that the maximum cross-section occurs at about 3° – 4° off the 0° aspect angle, whereas at the aspect angle of exactly 0° of the cross-section is zero, as already mentioned.

We have then successively increased the radar elevation angle β assuming that the centre of the scattering volume remains at 90-km altitude. The neutral wind, as well as the $\mathbf{E} \times \mathbf{B}$ drift was scaled by $1/\cos \beta$, thus assuming horizontal velocities of 34.6 m s^{-1} and 46.2 m s^{-1} ,

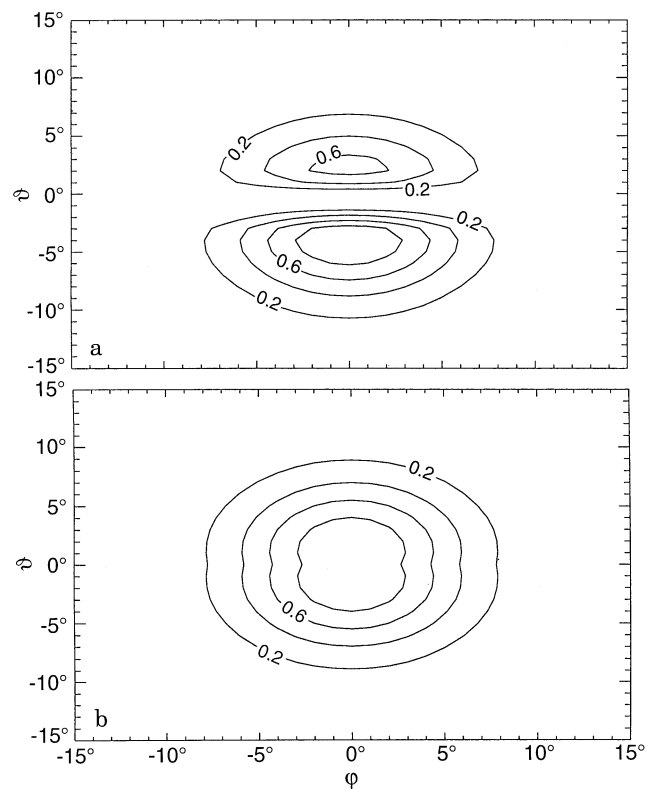


Fig. 5. **a** Integrand of Eq. 10, i.e. the antenna pattern folded with the backscatter cross-section as a function of the angles ϑ and φ for $k_{\text{par}}/k = 0.01$ and a radar elevation angle $\beta = 30^\circ$. **b** Same as **a**, but for a radar elevation of angle of 90° (vertical incidence)

respectively. The backscattered power ratio for our assumed antenna configuration as a function of the elevation angle is plotted in Fig. 4b. It reflects the aspect angle dependence already displayed in Fig. 4a, but also the increase in power towards vertical incidence because of the shorter range to the scattering volume. Therefore it varies only by a factor of about 2 over the studied elevation angle range compared to a factor of 40 over the corresponding aspect angle range. The shape of the spectrum does not change very much as a function of radar elevation. The width remains around 10 m s^{-1} as in the case of the cross-section (upper right-hand panel of Fig. 2). The backscatter cross-section folded with the antenna pattern for the case $\beta = 90^\circ$ is plotted in Fig. 5b; contrary to Fig. 5a it peaks in the direction of the radar beam.

Finally we have calculated the backscattered power as a function of radar frequency which can be expected with a 50-kW transmitter and the antenna described above. This result is plotted in Fig. 6 as a solid line. The dash-dotted line gives an estimate of the sky noise calculated from the equation

$$P_n = k_B T B_w, \quad (14)$$

assuming a receiver bandwidth $B_w = 50 \text{ kHz}$ ($k_B = \text{Boltzmann constant}$), and a sky noise temperature of $125\,000 \text{ K}$ at 10 MHz and 2000 K at 100 MHz (Kraus, 1986). This line crosses the backscattered power curve at

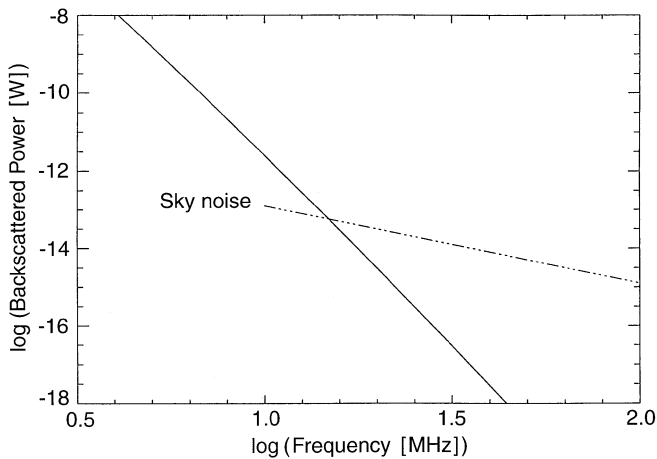


Fig. 6. Received backscatter power with the assumed antenna array and a transmitter power of 50 kW as a function of radar frequency. The dashed-dotted line gives an estimate of the sky noise

a frequency of about 15 MHz. Therefore at higher frequencies either pulse coding techniques, a higher transmitted power or a large antenna array have to be used in order to detect the echoes.

6 Concluding remarks

The rocket measurements cited in the introduction prove clearly that electron density fluctuations are present in the 80–100-km altitude range. According to our estimates the radar backscatter from these fluctuations should be likewise detectable with powerful radars, particularly at frequencies below 15 MHz. Indeed, MF-radar (2–4 MHz) observations (often cited as partial reflections) frequently show narrow spectra exhibiting a width of the order of 10 m s^{-1} , which was related to the characteristic velocity of the turbulence (e.g. Schlegel *et al.*, 1978; Manson *et al.*, 1981). The mean Doppler shift is usually interpreted as the neutral wind velocity (Gregory *et al.*, 1982; Manson *et al.*, 1990). Narrow spectra of a width up to 10 m s^{-1} have also been observed with the SURA facility in Nizhny Novgorod, Russia on 7–9 MHz (Karashtin *et al.*, 1996). So far these echoes have already been interpreted at least partly in terms of neutral turbulence. The fact that these echoes are stronger at middle and high frequencies was qualitatively explained in terms of the Kolmogorov spectrum: the scale lengths of the inertial subrange fit well to the wavelengths of such radars. This concept is incorporated in the theory of Gurevich *et al.* (1996) in quantitative terms (Eq. 3). It should be noted, however, that MF-radar echoes can partly be explained also by specular reflections from discrete layers (Röttger, 1980).

An important discrepancy between our estimates and the experimental backscatter results is the considerably larger received power. Although a quantitative estimate of the backscattered power is difficult and is rarely published for MF radars, it can be stated that they usually obtain strong echoes with less transmitter power and smaller antenna arrays than regarded here. The reason may be

that in this theory the turbulent medium has been treated as homogeneous and isotropic, which is probably a rather idealized assumption. Inhomogeneous and intermittent turbulence would yield higher backscattered power, but its theory has not yet been incorporated into this theoretical frame. Experimental indication of an isotropic medium is the fact that observed radar echoes are aspect sensitive around vertical incidence. Off-vertical backscatter is smaller by about $1\text{--}2 \text{ dB deg}^{-1}$ (Reid, 1988). This is another discrepancy in our results, where the backscattered power increases when the radar elevation angle deviates from the vertical direction ($\beta < 90^\circ$, see Fig. 4b). Note that the term aspect angle is used differently here compared to our discussion in Sect. 4.4. Here the deviation from the vertical direction is meant, rather than from the direction perpendicular to the magnetic field.

In conclusion, it should be stated that Gurevich *et al.* (1996) regard their theory as an important step into the direction of a quantitative treatment of plasma irregularities caused by neutral turbulence. Its further development and amendment with respect to the deficiency mentioned above is under way.

Acknowledgement. Topical Editor D. Alcayd  thanks T. A. Blix and C. Hanuise for their help in evaluating this paper.

References

- Blix, T. A., and E. V. Thrane, Experimental evidence for unstable long-wavelength waves in the lower E/upper D-region excited near the bisector between the electric field and the drift velocity, in *Plasma Instabilities in the Ionospheric E-Region*, Ed. K. Schlegel, Cuvillier Verlag, G ttingen, 1996.
- Blix, T. A., E. V. Thrane, S. Kirkwood, and K. Schlegel, Plasma instabilities in the low E-region observed during the DYANA campaign, *J. Atmos. Terr. Phys.*, **56**, 1853–1870, 1994.
- Buneman, O., Excitation of field-aligned sound waves by electron streams, *Phys. Rev. Lett.*, **10**, 285–287, 1963.
- Farley, D. T., A plasma instability resulting in field-aligned irregularities in the ionosphere, *J. Geophys. Res.*, **68**, 6083–6097, 1963.
- Gregory, J. B., C. E. Meek, and A. H. Manson, An assessment of wind data (60–110 km) obtained in real-time from a medium frequency radar using the radio wave drifts technique, *J. Atmos. Terr. Phys.*, **44**, 649–655, 1982.
- Gurevich, A. V., N. D. Borisov, and K. P. Zybin, Ionospheric turbulence induced in the lower part of the E-region by the turbulence of neutral atmosphere, *J. Geophys. Res.*, in press, 1996.
- Haldoupis, C., A review on radio studies of auroral E-region ionospheric irregularities, *Ann. Geophysicae*, **7**, 239–258, 1989.
- Hanuise, C., J. P. Villaine, D. Gresillon, B. Cabrit, R. A. Greenwald, and K. B. Baker, Interpretation of HF-radar ionospheric Doppler spectra by collective wave scattering theory, *Ann. Geophysicae*, **11**, 29–39, 1993.
- Hocking, W. K., Turbulence in the region 80–120 km, *Adv. Space Res.*, **10**(12), 153–161, 1990.
- Karashtin, A. N., Yu. V. Shlyugaev, V. I. Abramov, I. F. Belov, I. V. Berezin, V. V. Bychkov, E. B. Eryshev, and G. P. Komrakov, First HF-radar measurements of the mesosphere echoes at SURA, in *Plasma Instabilities in Ionospheric E-Region*, Ed. K. Schlegel, Cuvillier Verlag, G ttingen, 1996.
- Kelley, M. C., *The Earth's Ionosphere Plasma Physics and Electrodynamics* Academic Publ. Comp., San Diego, Cal., 1989.
- Kraus, J. D., *Radio Astronomy*, Cygnus-Quasar Books, Powell, Ohio, 1986.

- Lübken, F.-J., W. Hillert, G. Lembacher, and U. von Zahn**, Experiments revealing small impact of turbulence on the energy budget of the mesosphere and lower thermosphere, *J. Geophys. Res.*, **98**, 20369–20384, 1993.
- Manson, A. H., C. E. Meek, and J. B. Gregory**, Gravity waves of short period (5–90 min) in the lower thermosphere at 52°N (Saskatoon, Canada); 1978/1979, *J. Atmos. Terr. Phys.*, **43**, 35–44, 1981.
- Manson, A. H., C. E. Meek, M. Massebeuf, J. L. Fellous, W. G. Elford, R. A. Vincent, R. L. Craig, A. Phillips, R. G. Roper, G. J. Fraser, M. J. Smith, S. Avery, B. B. Balsley, R. R. Clark, S. Kato, T. Tsuda, R. Schmitter, and D. Kürschner**, Description and presentation of Reference Atmosphere radar winds (80–100 km), *Adv. Space Res.*, **10**(12), 267–315, 1990.
- Pfaff, R. F.**, Rocket observations in the equatorial electrojet: current status and critical problems, *J. Atmos. Terr. Phys.*, **53**, 709–728, 1991.
- Reid, I. M.**, MF Doppler and spaced antenna radar measurements of upper middle atmosphere winds, *J. Atmos. Terr. Phys.*, **50**, 117–134, 1988.
- Rinnert, K.**, Plasma waves observed in the auroral E-region – ROSE campaign, *J. Atmos. Terr. Phys.*, **54**, 683–692, 1992.
- Rose, G., K. Schlegel, K. Rinnert, H. Kohl, E. Nielsen, G. Dehmel, A. Frikker, F.-J. Lübken, H. Lühr, E. Neske, and A. Steinweg**, The ROSE project. Scientific objectives and discussion of first results, *J. Atmos. Terr. Phys.*, **54**, 657–667, 1992.
- Röttger, J.**, Reflection and scattering of VHF radar signals from atmospheric refractivity structures, *Radio Sci.*, **15**, 259–276, 1980.
- Røyrvik, O., and L. G. Smith**, Comparison of mesospheric VHF radar echoes and rocket probe electron concentration measurements, *J. Geophys. Res.*, **89**, 9014–9022, 1984.
- Schlegel, K.**, Measurements of electron density fluctuations during the ROSE rocket flights, *J. Atmos. Terr. Phys.*, **54**, 715–723, 1992.
- Schlegel, K.**, Coherent backscatter from ionospheric E-region plasma irregularities, *J. Atmos. Terr. Phys.*, **58**, 933–941, 1996.
- Schlegel, K., and A. V. Gurevich**, *Radar backscatter from E-region plasma irregularities induced by neutral turbulence*, Report MPAE-W-100-95-20, Max-Planck-Institut für Aeronomie, Katlenburg-Lindau, 1995.
- Schlegel, K., A. Brekke, and A. Haug**, Some characteristics of the quite polar D-region and mesosphere obtained with the partial reflection method, *J. Atmos. Terr. Phys.*, **40**, 205–213, 1978.
- Schlegel, K., E. C. Thomas, and D. Ridge**, A statistical study of auroral radar spectra obtained with SABRE, *J. Geophys. Res.*, **91**, 13483–13492, 1986.
- Simon A.**, Instability of a partially ionized plasma in crossed electric and magnetic fields, *Phys. Fluids*, **6**, 382–388, 1963.
- Sirovich, L., L. Smith, and V. Yakhot**, Energy spectra of homogeneous and isotropic turbulence in far dissipation range, *Phys. Rev. Lett.*, **72**, 344–347, 1994.
- Stubbe, P., H. Kopka, H. Lauche, M. T. Rietveld, A. Brekke, O. Holt, T. B. Jones, T. Robinson, A. Hedberg, B. Thide, M. Crochet, and H. J. Lotz**, Ionospheric modification experiments in northern Scandinavia, *J. Atmos. Terr. Phys.*, **44**, 1025–1041, 1982.
- Tatarski, V. I.**, *Wave propagation in turbulent medium*, Dover Publ. Inc., New York, 1961.